Acta Cryst. (1997). B53, 346–352

A New Structural Transformation Mechanism in Catalytic Oxides

PRATIBHA L. GAI

Central Research and Development, Science and Engineering Laboratories, DuPont, Experimental Station, Wilmington, DE 19880-0356, USA. E-mail: gaipl@esvax.dnet.dupont.com

(Received 4 September 1996; accepted 26 November 1996)

Abstract

During dynamic reduction of vanadyl pyrophosphate using *in situ* electron microscopy and diffraction under controlled reaction conditions, recurrent dislocation of atoms is observed, which leads to the formation of extended defects by a glide shear mechanism. Ordering of the glide shear defects leads to a new structure by transforming the orthorhombic vanadyl pyrophosphate into an anion-deficient tetragonal structure. These defects are formed close to the surface and the nature of the defects is such that they accommodate the misfit between the reduced surface layers containing anion vacancies and the underlying unreduced bulk. The glide shear planar defects (GS) essentially preserve anion vacancies and do not lead to a lattice collapse, and are distinct from the well known crystallographic shear planes (CS, which eliminate anion vacancies leading to lattice collapse). In important complex oxides such as vanadyl pyrophosphates, and in a variety of model ReO_3- and V_2O_5-based oxides used as catalysts, my *in situ* studies suggest that glide shear is the most effective defect mechanism by which the catalysts accommodate nonstoichiometry and continue to operate in partial oxidation reactions. Anion vacancy formation resulting from the oxide reduction is the driving force for the generation of glide misfit defects and their ordering can give rise to new phases or structures in oxides. The studies have important implications in oxide catalysis and, more generally, in oxide crystallography.

1. Introduction

Oxides are widely exploited as catalysts in the selective oxidation of hydrocarbons. Catalytic oxides exchange oxygen with oxygen gas and provide lattice oxygen in catalytic oxidation reactions. Structural changes in these oxides are of considerable scientific and technological importance. They are directly relevant to central issues such as performance and stability of oxides in chemical, material sciences and technological applications. For the early transition metal oxides (*MO*, such as molybdenum oxides, vanadium oxides and titania), which consist of blocks of MO_6 octahedra as their basic structural unit, changing their anion content introduces considerable structural rearrangement. Some of the recognized ways by which oxides accommodate nonstoichiometry and changes in composition are crystallographic shear [CS, which essentially eliminates complete planes of anion vacant sites by shear from corner to edge sharing of octahedra and lattice collapse (Magneli, 1953, 1970; Wadsley, 1964, Andersson & Wadsley, 1965)], coherent intergrowths (Anderson, 1972) and compositional twinning (Bakker & Hyde, 1978; Bursill & Hyde, 1972). These have been investigated extensively in the literature using a variety of techniques, including electron microscopy, generally on static post-reaction samples (reacted *ex situ* and cooled to room temperature) held in high vacua. However, studies on static samples do not represent dynamic catalytic oxide surfaces which evolve during redox processes and this has hindered a better fundamental understanding of mechanisms leading to structural transformations. To understand the nature and role of structural changes in reacting oxides the first direct studies of dynamic catalytic reactions under controlled conditions of temperatures and reducing and oxidizing gas environments were undertaken using *in situ* dynamic electron microscopy, on simple model oxide catalysts such as MoO_3 (Gai, 1981; Gai & Labun, 1985), V_2O_5 (Gai, 1983) and related oxides (Gai, Smith & Owen, 1990, 1992, 1993). These direct studies have shown that at higher operating temperatures of ~ 673 K crystallographic shear planes (CS) are formed. However, the dynamic microstructural studies correlated with reaction chemistry showed the CS planes to be consequences of catalytic reactions, eliminating supersaturation (SS) of anion vacancies (SS defined as that relative to the background concentration of vacancies in equilibrium with CS planes). They were secondary (or detrimental) to catalysis since selectivity to desired products decreased in the presence of CS planes in partial oxidation of hydrocarbons and were not the origin of activity in oxygen exchange in redox processes (Gai, 1981, 1992, 1993). The question therefore arises as to the possibilities of novel, alternative but effective mechanisms to accommodate nonstoichiometry in oxides employed as catalysts. The objective of the present work is to explore structural transformations in scientifically and technologically important vanadyl pyrophosphate mixed-metal complex oxides during

reactions. In this paper the structural transformation mechanism by a misfit glide shear process leading to a new structure is revealed. Furthermore, the results indicate that the glide shear process can be beneficial in catalytic partial oxidation reactions.

2. Experimental

Vanadyl pyrophosphates [$(VO)_2P_2O_7$, hereafter referred to as VPO] were prepared according to an established organic route using vanadium pentoxide, anhydrous phosphoric acid, in isobutyl alcohol, and benzyl alcohol (Gai, 1992; Gai & Kourtakis, 1995). VPO is the most successful catalyst used in *n*-butane oxidation technology to produce maleic anhydride [MA (Hodnett, 1985; Bordes, 1987; Centi, 1993)], with end uses in furans. Dynamic reduction and partial oxidation reactions of the catalyst in reducing and oxidizing environments from room temperature to an operating temperature of ~ 673 K were probed directly using our novel environmental cell-high-resolution electron microscope (EHREM) under controlled gas environments and temperatures (Boyes & Gai, 1996; Gai, Kourtakis, Coulson & Sonnichsen, 1997). In EHREM a microreactor (environmental cell) is placed inside the column of a Philips CM30 high-resolution electron microscope (EM). The method has made it possible to observe dynamic (live) gas–solid catalytic reactions directly (*in situ*) at the atomic scale, capture and record dynamic events in real time and to maintain electron diffraction capabilities. The *in situ* technique is very powerful for studying dynamic surface as well as bulk phenomena. Both EHREM and parallel reaction chemistry tests were performed in reducing environments of butane, hydrogen as well as in nitrogen and partially oxidizing 1.5% butane–air environments at ~ 673 K.

3. Results and discussion

It is generally accepted that the structure of VPO is orthorhombic with $a = 16.594$, $b = 7.76$ and $c = 9.588$ Å (Gorbunova & Linde, 1979). An idealized structural model of VPO in the (010) orientation is shown in Fig. 1(*a*). Double chains of edge-sharing vanadium octahedra (VO_6) are linked by phosphate tetrahedra in (010). Our systematic experimental observations are presented in Figs. 1(*b*)–4. The samples which are electron-beam-sensitive were examined under very low beam currents in EHREM using a low light-level television camera and a video system. Blank experiments (without the beam) were also carried out on samples (with the beam switched on for a few seconds for recording) to confirm the dynamic studies. Under the low beam currents used, no beam damage was detected in the dynamic experiments. An EHREM lattice image of (010) VPO in butane at room temperature is shown in Fig. 1(*b*), with the associated electron diffraction (ED) inset. The structural model shown in Fig. 1(*a*) is approximately superimposed onto the lattice image to illustrate vanadyl-dimer and P-atom column positions in the unit cell. The lattice image and the ED show a well ordered structure and sharp Bragg reflections. A low-resolution image of VPO crystals showing a 'rosette' morphology is also inset.

The dynamic reduction of the VPO catalysts in EHREM in butane at the catalyst-operating temperature of ~ 673 K showed two sets of extended defects in diffraction contrast and in HREM, along the two

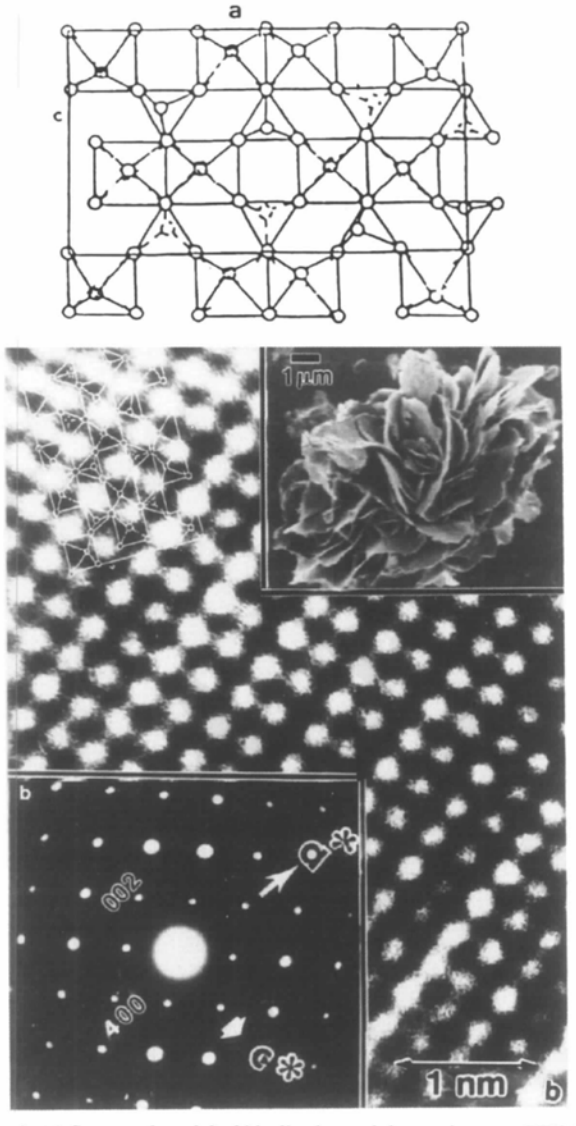

Fig. 1. (*a*) Structural model of idealized vanadyl pyrophospate (VPO) in (010) planar projection. Vanadyl octahedra and phosphate tetrahedra are interlinked. (*b*) EHREM lattice image in butane of fresh VPO in (010). The associated ED is inset and the structural model from (*a*) is approximately superimposed and dark regions illustrate columns of vanadyl dimers and P atoms. The lattice image and ED show well ordered structure. Morphology is inset.

symmetry-related [201] and [20$\bar{1}$] directions in the early stages of reduction, in an otherwise clean VPO matrix. The defects along the two directions make an angle of ~80° with one another and the lattice spacing [d(201)] is ~ 6.26 Å. Under the reducing conditions of butane there is a large driving force for the generation of anion vacancies following lattice oxygen loss. The defects were observed to nucleate close to the surface following

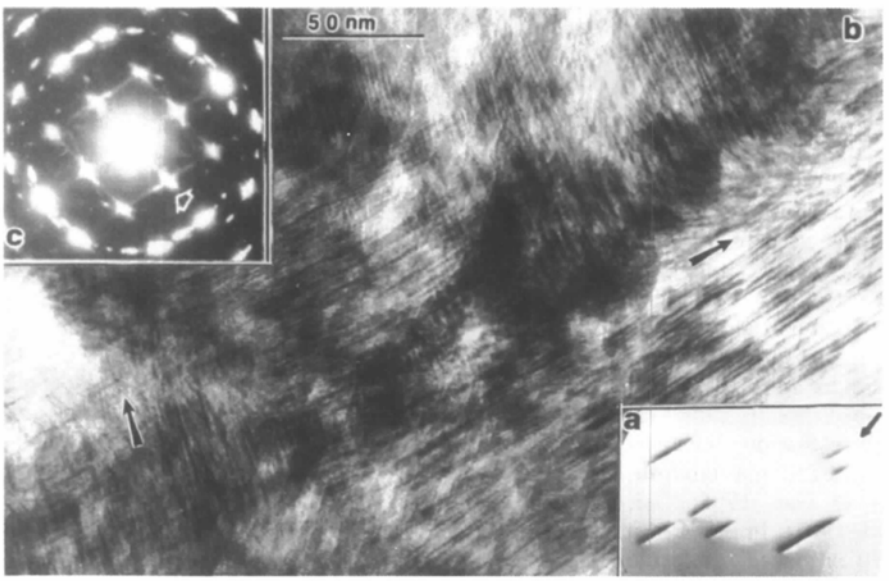

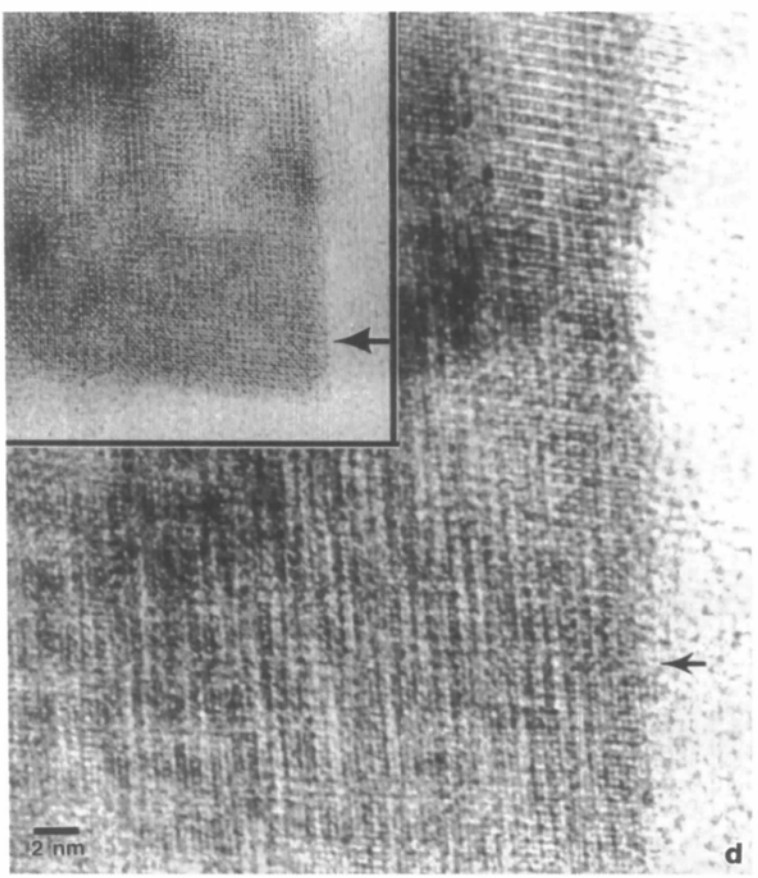

Fig. 2. Direct studies of VPO reduction in butane at 673 K. (*a*) One set of dynamic extended defects formed close to the surface, imaged in the 201 reflection. (*b*) Both sets of defects along symmetry-related [201] and [201] directions shown by arrows. This creates ~80° between one another (~ 673 K, after reduction of several hours). (*c*) The corresponding ED with diffuse streaks along ⟨201⟩ (arrowed) as an inset. (*d*) One set of defects in high resolution. The inset shows crystal area magnified in (*d*).

reduction in a couple of minutes and extend throughout the bulk as a function of reduction time. Fig. 2(*a*) shows one set of dynamic defects near the surface in a 201 reflection and (*b*) shows both sets of defects (arrowed) along the two ⟨201⟩ directions, imaged in the 400 reflection after several hours of reduction at ~ 673 K. The associated electron diffraction (*c*) shows two sets of diffuse streaks (arrowed) along ⟨201⟩ originating from the defect strain fields.

The streaks suggest that the extended defects are not ordered. One set of defects in high resolution is shown in Fig. 2(*d*), magnified from an area of the crystal (near the arrow) shown in the inset. Defects (dislocations in lattice) are characterized by displacement vectors (**b**). To determine the nature and magnitude of **b** associated with the defects we have used the conventional diffraction contrast (imaging with single Bragg reflection), with HREM, to determine the components of **b** in all the x, y and z crystal directions (Hirsch, Howie, Nicholson, Pashley & Whelan, 1985). Briefly, the intensity (contrast) of the defect is mapped in several reflections (Gai & Kourtakis, 1995) by tilting the crystal to different reflections (**g**) in EHREM ($\mathbf{g} \cdot \mathbf{b}$ dot product analysis), including the reflection in which it is invisible, $\mathbf{g} \cdot \mathbf{b} = 0$ when g is normal to the reflecting planes. Defects showed no contrast in 010 and in the important symmetry-related 201 and $20\bar{1}$ reflections, indicating zero component along the y direction, with **b** parallel to the line of the defect, confirmed by HREM. The detailed analysis showed the defects to be formed by a novel glide shear mechanism. For example, defects in 201 (Fig. 3*a*) and $20\bar{1}$ reflections (Fig. 3*b*), taken from the same area near A, reveal that the displacement vector associated with the defects lies in the plane of shear (with no lattice collapse). From the analysis the displacement vector is deduced to be $\pm\langle a/7, 0, c/4\rangle$ and the character is very close to screw dislocations. These experiments and the corresponding intensity calculations of defects in Fig. 2(*a*) have indicated that the defects are partial dislocations formed close to the surface at a depth of a few (~3–4) nanometers.

The formation of the defects was also observed by heating the oxide in H_2 and N_2 environments. The reasons for the formation of the glide defects can be understood as follows. The dynamic studies in butane, H_2 and N_2, leading to the defects, show that during reduction anion vacancies are introduced into the crystal. The anion vacancies lie in the basal plane between corner-sharing vanadyl octahedra and phosphate tetrahedra. To accommodate the minimization of the accompanying strain energy, these defects are generated by simple crystal glide to accommodate the misfit between the reduced surface layers containing anion vacancies and the underlying unreduced bulk. Fig. 4(*a*) is a schematic illustration of the proposed mechanism of the glide shear process observed in our experiments. The defects thus arise because of a slightly anion-deficient vanadyl pyrophosphate and the glide process accommodating the crystal misfit at the interface between the surface and the bulk helps to preserve anion vacancies (V^{3+} phases). These local glide defect regions do not change the overall VPO structure pattern in X-ray diffraction due to peak overlap (discussed below) and therefore these local changes are not clearly visible in X-ray diffraction data. Specifically, *in situ* electron microscopy and electron diffraction have been essential to observe the important defect reaction mechanism.

The defects are partial dislocations in the perfect structure separating a stacking fault in {201} planes and the stacking fault is terminated by the dislocation (Fig. 4*b*). Models used to interpret the glide defects and the growth of lower-energy (201) crystal faces are shown in Fig. 4(*c*), and of the misfit glide defect at the interface between reduced surface layers containing anion

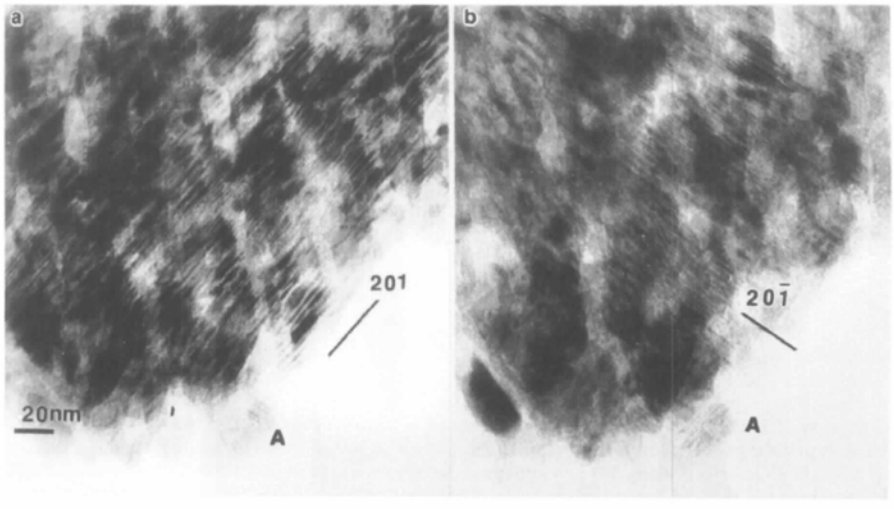

Fig. 3. Diffraction contrast images of defects from the same area A of the crystal: (*a*) 201 and (*b*) $20\bar{1}$ reflections show that the displacement vector lies in the plane of shear and indicate a glide shear mechanism.

vacancies and VPO bulk are shown in Fig. 4(*d*). Selectivity to maleic anyhdride for successive butane pulses measured in the absence of air showed a MA selectivity of ~60% initially and achieved a steady rate at ~52% after a few hours. In partial oxidation with 1.5% butane–air selectivity to MA was measured to be high and nearly uniform 80% selectivity at ~20–60% butane conversion. It is possible to maintain this high selectivity for prolonged periods. The result in the partial oxidation showing uniform selectivity indicates that because the vacant anion sites (which change the strength of Lewis acid sites) are readily available as active sites for oxygen exchange, oxidation (regeneration) of the catalyst can proceed more quickly than in the presence of CS planes which eliminate such vacant sites. The faster regeneration of the catalyst can prolong its operational life.

The defect concentration was found to increase with increased reduction. In samples reduced for several days at 673 K repeated glide shear and ordering to a crystallographically defined anion-deficient compound with a plate morphology was observed in electron diffraction and imaging. Fig. 5(*a*) shows the plates along the ⟨201⟩ defect directions (some microcrystallinity within the plates was sometimes found). Some quite well formed plates in other orientations are shown in Fig. 5(*b*). ED from various crystallographic orientations from the plates were recorded by tilting the plates to different crystal zone axes and are summarized in Figs. 5(*c*) and (*d*). It may be noted that some lattice disorder (streaking) is still visible along the original $[201]_{VPO}$ direction. From the electron diffraction measurements the new transformed structure is deduced to be tetragonal with the lattice parameters $a \simeq 7.8$ and $c \simeq 6.3$ Å. The ED patterns in Figs. 5(*c*) and (*d*) are from the [010] and [100] zone axes and are indexed based on the new tetragonal cell parameters. There is excellent agreement between the experimental measurements and calculations of lattice spacings and angles of different $\{hkl\}$ planes in the new tetragonal lattice. In X-ray diffraction (200) and (201) VPO reflections overlap with (200) and (001) reflections of the tetragonal plates, respectively. Superposition and broadening of other peaks are also

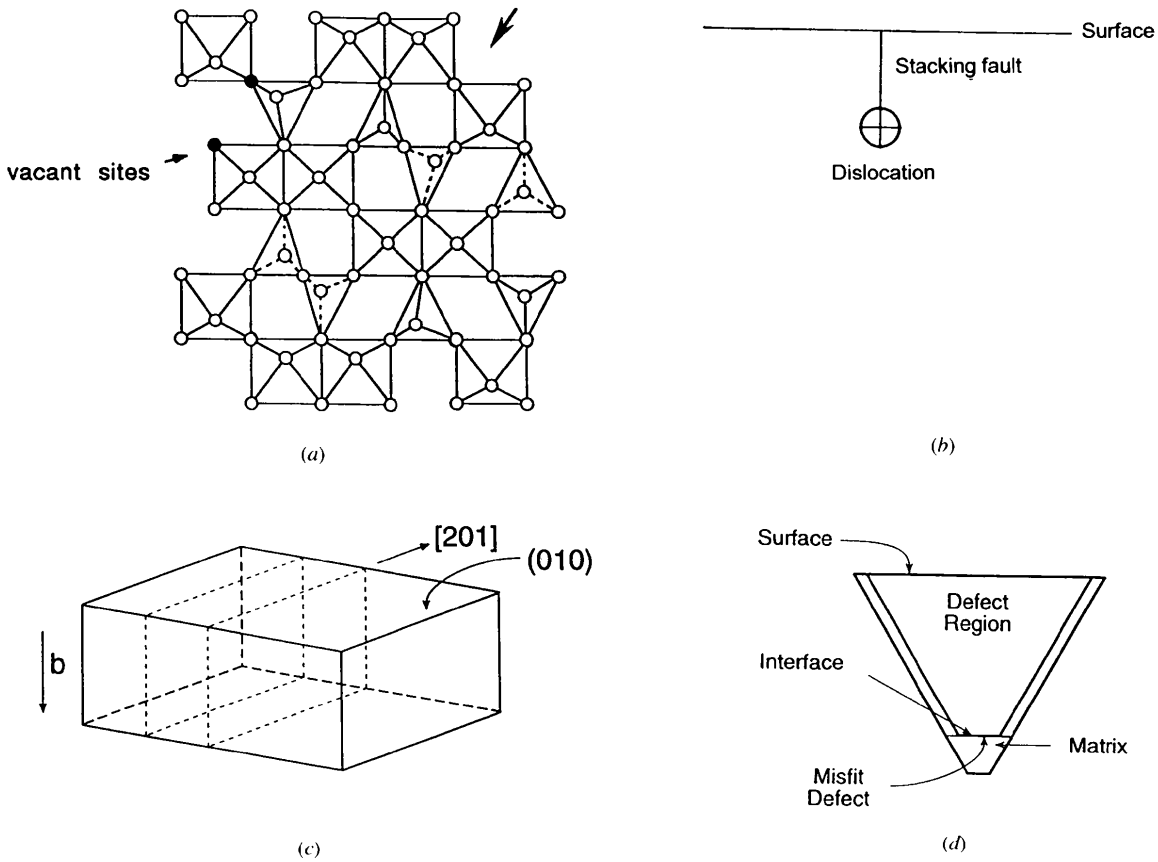

Fig. 4. (*a*) A model for glide shear based on *in situ* EHREM data. Projection of one layer of idealized VPO on (010), indicating a glide shear along ⟨201⟩ (arrowed). (*b*) Model used to interpret the glide defects formed close to the surface: A partial screw dislocation bounds a stacking fault extending to the surface. (*c*) Model of misfit glide defects along 201 and growth of the 201 crystal faces. (*d*) Model of glide shear defects accommodating misfit strains at the interface between reduced oxide surface layers containing anion vacancies and the underlying bulk.

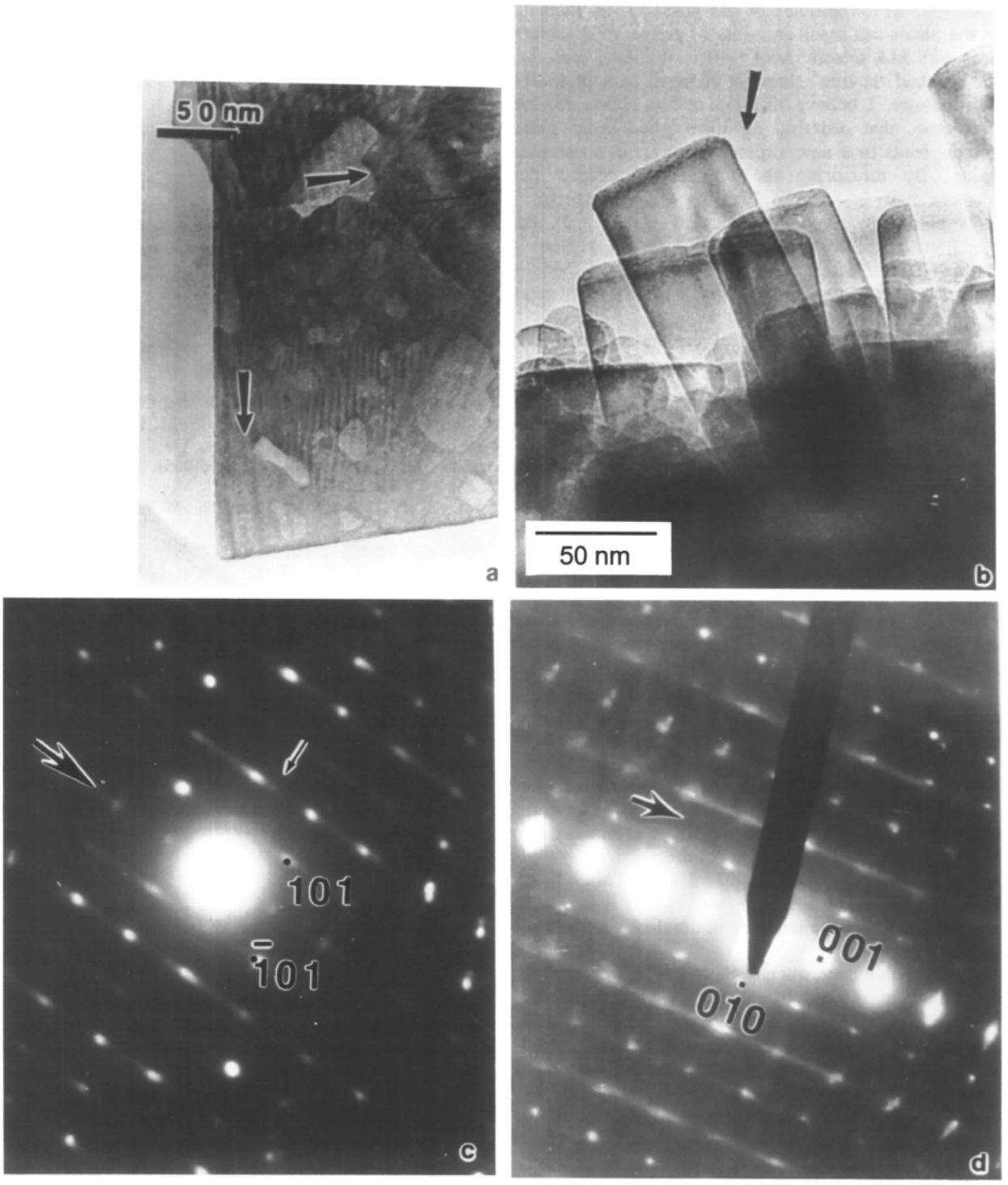

Fig. 5. Prolonged reduction of VPO at 673 K: (*a*) plate formation along ⟨201⟩. (*b*) Quite well formed small plates showing VPO rosette morphology is changed to an anion-deficient plate morphology. The ED data shown in (*c*) and (*d*) indicate structural transformation of orthorhombic VPO to tetragonal plate crystals of $VPO_{4.33}$: (*c*) tetragonal anion-deficient V—P—O in the [010] zone axis. Some lattice disorder along the original $[201]_{VPO}$ (misfit glide shear defect directions) is still evident and the evolution of faint 200 (small arrow) and 101 reflections can be seen in the partially ordered crystal. (*d*) Tetragonal V—P—O in the [100] zone axis. Some lattice disorder along the original $[201]_{VPO}$ is still partly evident. The lattice parameters deduced are $a \simeq 7.8$ and $c \simeq 6.26$ Å. In X-ray diffraction, peak overlap is observed.

observed. In the absence of gas phase O_2 an increase in the plates can result in a loss of active VPO surface area with MA selectivity of ~40%. It can be seen that the original 'rosette' shape is changed to a plate-like morphology. I believe that the results show, for the first time, that ordering of misfit glide shear plane defects leads to a new structure (phase) in a catalytic oxide. By measuring the number of defects per formula unit (*e.g.* from Fig. 2, ~2 defects per 7 units giving an anion deficiency of $\sim 0.15 \times 2$), the oxidation state of V in the local defect region is estimated as ~ 3.7. The defective phase then is approximately $(VO)_2P_2O_{6.67}$, which can be written as $V_nP_nO_{4n+1}$ for $n = 3$.

The glide shear plane defect mechanism described here is distinct from the CS plane mechanism. In the glide shear process observed during the reduction of VPO the local lattice structure is not collapsed, only local symmetry is altered (in antiphase), as shown in Fig. 4(*a*). However, the glide shear plane defects are nucleated only when the catalyst is slightly reduced and the crystal simply glides along ⟨201⟩ to accommodate misfit strains between anion-deficient surface layers and the unreduced bulk. The energy requirement for the proposed glide shear mechanism is much less than that for a CS plane which eliminates lattice sites in supersaturation and causes lattice collapse. The defects described here have an almost pure shear (screw) character and they can be nucleated as small shear loops in the presence of large shear strains arising because of a slight reduction of the catalyst surface. The loops can expand through a glide mechanism that is driven by lattice strain.

Notably, my *in situ* EM studies of the reduction of model catalytic oxides such as MoO_3, V_2O_5 and related oxides at moderate temperatures, 473–623 K, have also shown structural transformation of these oxides by glide shear (Gai, 1981, 1983, 1992, 1993). These lower temperatures where the glide mechanism is operative are found to be beneficial for optimal catalyst performance.

The dynamic experiments show that although the CS mechanism pioneered by Magneli (1953, 1970) and Wadsley (1964) has been structurally highly elegant, in important applications such as catalysis glide shear is likely to be the most effective defect mechanism for accommodating nonstoichiometry. In addition, the key observation of glide shear in the *in situ* studies could provide a means for synthesizing novel oxide structures and novel phases for catalysis by suitable substitutions to induce selective glide transformations.

In summary, a new structural transformation mechanism by crystal glide shear is revealed with important implications in oxide catalysis and oxide crystallography. The mechanism is based on the glide defects relieving misfit strains between reduced oxide surface layers and the bulk, and may provide active sites for catalysis. Ordering of the glide shear plane defects transforms orthorhombic VPO into a tetragonal structure.

I would like to thank L. G. Hanna for technical support, and E. D. Boyes and K. Kourtakis for helpful discussions. My early *in situ* electron microscopy work on model systems was started at the University of Oxford, England, and I thank the technical support staff at the University.

References

Anderson, J. S. (1972). *Surface and Defects in Solids*, edited by M. W. Roberts, Vol. 1, pp. 19–31. London: Chemical Society.

Andersson, S. & Wadsley, A. D. (1965). *Nature*, **211**, 581–583.

Bakker, M. & Hyde, B. G. (1978). *Philos. Mag.* **38**, 615–628.

Bordes, E. (1987). *Catal. Today*, **1**, 499–511.

Boyes, E. D. & Gai, P. L. (1996). *In-Situ Electron and Tunneling Microscopy of Dynamic Processes*, edited by R. Sharma, P. L. Gai, M. Gadjardziska, R. Sinclair and L. Whitman, Vol. 404, pp. 53–60. Pittsburgh, USA: Materials Research Society.

Bursill, L. & Hyde, B. G. (1972). *Prog. Solid State Chem.* **7**, 177–198.

Centi, G. (1993). *Catal. Today*, Special Volume, **16**, 1–119.

Gai, P. L. (1981). *Philos. Mag.* **43**, 841–855.

Gai, P. L. (1983). *Philos. Mag.* **48**, 359–371.

Gai, P. L. (1992). *Catal. Rev. Sci. Eng.* **34**, 1–54.

Gai, P. L. (1993). *J. Solid State Chem.* **104**, 119–130.

Gai, P. L. & Kourtakis, K. (1995). *Science*, **267**, 661–663.

Gai, P. L. & Labun, P. A. (1985). *J. Catal.* **94**, 79–96.

Gai, P. L., Kourtakis, K., Coulson, R. & Sonnichsen, G. (1997). In *Catalysts for High Temperature Processes*, edited by K. Ramesh, M. Misono & P. L. Gai (-Boyes), in the press. American Ceramic Society.

Gai, P. L., Smith, B. C. & Owen, G.(1990). *Nature*, **348**, 430–432.

Gorbunova, Y. E. & Linde, S. A. (1979). *Dokl. Acad. SSSR*, **245**, 584–592.

Hirsch, P. B., Howie, A., Nicholson, R., Pashley, D. & Whelan, D. J. (1985). *Electron Microscopy of Thin Crystals*. Malabar, Florida, USA: Krieger.

Hodnett, B. G. (1985). *Catal. Rev. Sci. Eng.* **27**, 373–395.

Magneli, A. (1953). *Acta Cryst.* **6**, 495–500.

Magneli, A. (1970). *The Chemistry of Extended Defects*, edited by L. Eyring & M. O'Keefe, pp. 148–163. Amsterdam: North Holland.

Wadsley, A. D. (1964). *Nonstoichiometric Compounds*, edited by L. Mendelcorn, Vol. 1, pp. 98–110. New York: Academic Press.